ChemPubSoc Europe

DOI: 10.1002/slct.201801611

Chemistry SELECT Full Papers

Materials Science inc. Nanomaterials & Polymers

Vibrational Signatures of Calcium Oxalate Polyhydrates

Ivan Petit,[a] Gustavo D. Belletti,[b] Théau Debroise,[a] Manuel J. Llansola-Portoles,[c] Ivan T. Lucas,[d] César Leroy,[a] Christian Bonhomme,[a] Laure Bonhomme-Coury,[a] Dominique Bazin,[a] Michel Daudon,[e, f] Emmanuel Letavernier,[e, f] Jean Philippe Haymann,[e, f] Vincent Frochot,[e, f] Florence Babonneau,[a] Paola Quaino,[b] and Frederik Tielens*[a, g]

The vibrational signatures of the calcium oxalate polyhydrates are investigated using a combination of Density Functional Theory-Dispersion corrected, Fourier Transform- Raman and -Infrared (IR) spectroscopies. Most vibrational bands were assigned and the theoretical predictions were compared with in-house and other experimental data, for both, IR and Raman spectroscopies. Such an approach allowed a more accurate analysis of vibrational spectra helping in the completion of the band assignments of the vibrational bands of the mono, di, and tri hydrate calcium oxalate (COM, COD, and COT). Particular attention has been paid to the degree of hydration of COD, the low Raman wavenumbers, and the presence of oxalic acid in natural calcium oxalate polyhydrates. The obtained results are expected to be supportive in the detection of the different polyhydrates in natural samples, such as in kidney stones.

Introduction

Fourier Transform (FT)-Raman and (FT)-Infrared spectroscopies constitute significant tools for bio-medical diagnoses.[1] Two different approaches are at the present investigated to implement these techniques into the regular diagnosis apparatus. The first one is based on statistical analyses of the vibrational spectra. This approach has been used to study the disorder and variations in composition as well as in the crystal structures of deposits in the tissues.[2] This methodology has been explored for a wide range of pathologies, however only a few are routinely used into applications at the hospital.[3] A major weakness of the implementation of a statistical approach is mainly due to the fact that significant variations in the IR spectrum can be caused by subtle changes in the preparation procedure.[4] Another reason is related to the need for a precise analysis of the shape and the position of absorption bands for these two spectroscopies.[5] At the moment, one of the few applications is to establish medical diagnosis for kidney stones [6] and ectopic calcifications.[7] Recently, selected results regarding these research themes, as well as recent experimental developments, such as the ability to perform nanometer scale near-field infrared microscopy[8] provided relevant data in this field.[3]

Due to recent technical developments in laboratory apparatus, IR spectroscopy can be implemented at sub-cellular scale in a time frame of seconds to milliseconds. This is of major importance due to the amount of samples to be collected and more than 75,000 kidney stones and 1,100 biopsies have been already characterized at the Necker and Tenon hospitals using the described techniques. The data bank created from those measurements facilitates epidemiologic studies for the clinician to relate urolithiasis to other major public health problems such as type II diabetes.[9]

On the contrary, Raman spectroscopy is not routinely used at the hospital for microcrystalline pathologies, mainly because it has some disadvantages compare to IR spectroscopy. For example, in the case of sub-micrometer crystals, the Raman probe, i.e. the excitation laser, can modify the chemistry of the deposit through heat dissipation. In addition, the tissue may display a significant background signal (Raman signature and/or auto-fluorescence) which can impact on the reliability of the detection of deposits with low Raman scattering cross section. The signal to noise ratio can however be improved through suitable tuning of the excitation laser wavelength from visible to near-IR.

However, Raman shows also major advantages compare to IR spectroscopy. Compositional mapping of samples simply deposited on supports used routinely at the hospital, i.e. glass,

[a] *Dr. I. Petit, T. Debroise, Dr. C. Leroy, Prof. C. Bonhomme, Dr. L. Bonhomme-Coury, Dr. D. Bazin, Dr. F. Babonneau, Prof. F. Tielens*
Sorbonne Université, CNRS, Collège de France, Laboratoire de Chimie de la Matière Condensée de Paris, LCMCP, F-75005 Paris, France
E-mail: frederik.tielens@upmc.fr
[b] *Dr. G. D. Belletti, Prof. P. Quaino*
Instituto de Química Aplicada del Litoral, IQAL (UNL-CONICET), PRELINE (FIQ-UNL), Universidad National del Litoral, Santa Fe, Argentina
[c] *Dr. M. J. Llansola-Portoles*
Institute for Integrative Biology of the Cell (I2BC), CEA, CNRS, Université Paris-Saclay, F-91198, Gif-sur-Yvette cedex, France
[d] *Dr. I. T. Lucas*
Sorbonne Université, CNRS, Laboratoire Interfaces et Systèmes Electrochimie, LISE, F-75005 Paris, France
[e] *Dr. M. Daudon, Prof. E. Letavernier, Prof. J. P. Haymann, Dr. V. Frochot*
UMR S1155, INSERM/UPMC, 4 Rue de la Chine, 75970 Paris Cedex 20, France
[f] *Dr. M. Daudon, Prof. E. Letavernier, Prof. J. P. Haymann, Dr. V. Frochot*
AP-HP, Hôpital Tenon, Explorations fonctionnelles multidisciplinaires, 4 Rue de la Chine, 75970 Paris Cedex 20, France
[g] *Prof. F. Tielens*
General Chemistry (ALGC), Vrije Universiteit Brussel (Free University Brussels-VUB), Pleinlaan 2, 1050 Brussel, Belgium

Supporting information for this article is available on the WWW under https://doi.org/10.1002/slct.201801611

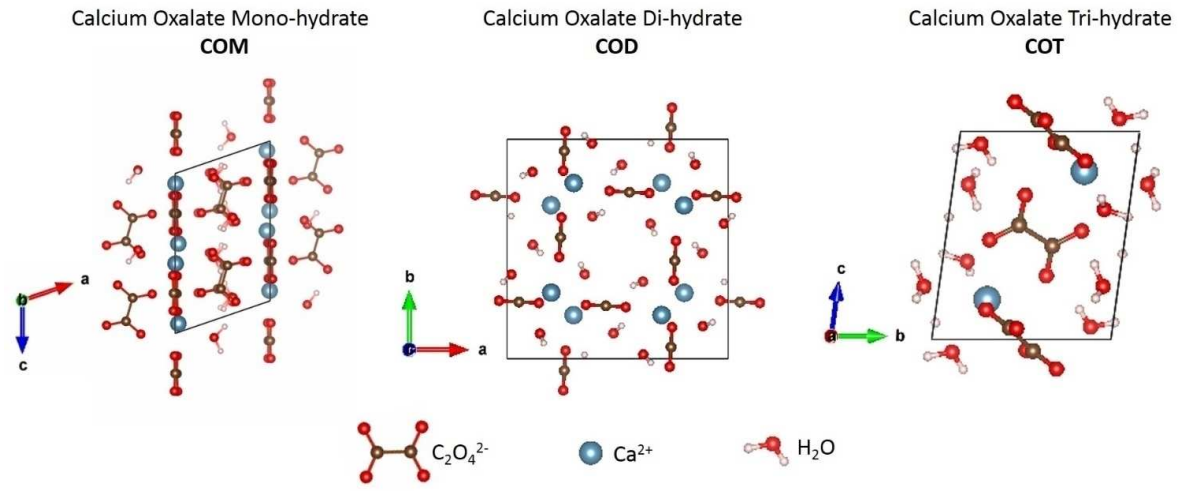

Figure 1. Unit cells of the three calcium oxalate polyhydrates, whewellite (COM), weddellite (COD), and caoxite (COT). The zeolitic water in the COD structure is not shown for clarity.

Table 1. Experimental and calculated unit cell parameters for the three calcium oxalate polyhydrates, COM, COD, and COT. Distances in Å, and angles in degrees.

Unit cell parameter	Experimental			PBE–D2			PBE–D3		
	COM[17]	COD[11]	COT[24a]	COM	COD	COT	COM	COD	COT
a	6.32	12.37	6.01	6.31	12.43	6.13	6.36	12.64	6.20
b	14.54	12.37	7.15	14.58	12.42	7.10	14.84	12.62	7.13
c	10.12	7.36	8.43	10.10	7.35	8.37	10.28	7.46	8.54
α	90.00	90.00	76.54	90.00	89.99	75.80	90.00	90.10	76.20
β	109.00	90.00	70.30	109.56	89.84	69.86	109.50	89.80	69.60
γ	90.00	90.00	70.75	90.01	90.95	69.91	90.00	90.90	69.30
average deviation (%) of a,b,c from exp	-	-	-	0.21	0.34	1.14	1.43	1.85	1.58

can be easily obtained with a sub-micron resolution. Measurements through glass cover slips protecting air sensitive samples are also possible. In addition, in Raman the 50 cm^{-1} to 400 cm^{-1} spectral range is accessible even down to 10 cm^{-1} with enhanced filtering of the laser line, providing precise (unambiguous) chemical signature of the sample under scrutiny.

The use of IR or Raman spectroscopy as diagnostic tools at the hospital ideally presupposes a complete understanding of the origin of the absorption (IR) or scattering (Raman) bands of pathological deposits. This is achievable through the calculation of theoretical ab *initio IR and Raman spectra of the different constituting compounds*. The complete characterization of the spectra is of utmost importance in the identification for the calcium oxalate compounds present in more than 70% of the kidney stones, and in numerous tissue calcifications.

By computing, at the Density Functional Theory-Dispersion (DFT–D) level, the IR and Raman vibrational spectra of the polyhydrates of the calcium oxalates: whewellite (monohydrate: COM), weddellite (dihydrate: COD), and caoxite (trihydrate: COT), we provide data that can be used to identify/quantify the different polyhydrates in natural mixtures such as in biological calcifications or kidney stones.

In this work, the theoretical predictions are compared with the available experimental data, for both, IR and Raman spectroscopies allowing the assignment of the most relevant vibrational bands of calcium oxalate polyhydrates.

Results and discussion

Structural analysis

The unit cell coordinates and parameters of the calcium oxalate polyhydrates were optimized at the PBE–D2 or the PBE–D3 level. The corresponding parameters are shown in **Figure 1** and the unit cell parameters are shown in **Table 1**.

COM, $CaC_2O_4{\cdot}H_2O$ (also known as whewellite) is the most abundant calcium oxalate (66%) phase found in kidney stones.[10] This chemical phase has been studied in the past by numerous groups, both experimentally[11] and theoretically.[12] The COM phase crystallizes in the monoclinic crystalline system with the space group $P2_1/c$. In 1965, Arnott et al.[13] solved the structure of the COM phase, extracted from the stem and leaves of Yucca rupicola, by X-rays. Although containing many impurities, crystals of sufficient size (200 μm) could be selected for a single crystal study, which was not possible with the

previous synthetic samples. More recently, several studies have helped to refine the structural parameters of the COM, in particular those from Tazzoli et al.,[14] Hochrein et al.,[15] and Deganello et al..[16] These investigations have established COM structures at different temperatures and have shown that there can be a reversible change in space group from $P2_1/c$ to I2/m at 328 K. Finally, a neutron diffraction study by Daudon et al.[17] on a single crystal of COM allowed to locate the proton positions of the water molecules of the structure. Therefore, this structure has been chosen as the starting geometry for our calculations.

The COD phase is commonly found in kidney stones but is also present as sediment in the Weddell Sea in Antarctica hence its name: weddellite.[18] Its structure has the particularity of presenting zeolitic channels. These channels allow adsorption of large quantities of water molecules that can diffuse 'freely' in the structure. These molecules should not be confused with the 'crystalline' water which is an integral part of the structure. Indeed, the COD phase formula is $CaC_2O_4{\cdot}(2+x)H_2O$, where x represents the amount of water present in the zeolitic channels ($x < 1$). Even now, the number of water molecules within the structure is subject to discussion. In 1964, Sterling proposed a structure for this phase and addressed the problem of defining the number of water molecules contained in the whole structure.[18–19] He established that the weddellite crystallizes in the tetragonal system with I4/m space group. He also determined the positions and partial occupations of oxygen associated with these water molecules. Tazzoli and Domenegetti[14] later refined the structure and determined an x value of 0.37, which is retained in this study (corresponding to 3 extra water molecules in the COD unit cell). The disorderly nature of the water molecules along the z axis has been demonstrated with the separation of the positions of oxygen atoms in two sites by crystallographic studies. Based on the refinements of the structures of kidney stones by Izatulina et al.[20] and by Tazzoli and Domenegetti,[14] Izatulina et al.[21] estimated an x value ranging from 0.13 to 0.37.

Additionally, COD is a metastable phase that turns into COM if it is not kept under certain conditions: Conti et al. have followed this transformation by X-ray diffraction and IR[22] suggesting that the presence of this phase in kidney calcification is promoted by the environment in which it evolves.

The COT trihydrate phase also called caoxite is the least common of the three calcium oxalate hydrates.[23] With the chemical formula $CaC_2O_4{\cdot}3H_2O$, it presents a triclinic structure with space group $P\bar{1}$. Its name is derived from the acronym for CAlcium OXalate and Centennial Anniversary Of X-rays and was proposed on the occasion of centenary of X-ray diffraction.[24] Deganello et al.[25] were the first to determine the structure for COT which existence had previously been suspected by Walter-Levy and Laniepce,[26] and Gardner.

First proposed as an intermediary in the formation of forms COM and COD in kidney stones,[23,27] this hypothesis has since been abandoned in favor of that of an amorphous phase of calcium oxalate as a precursor.[28] Although, rarely reported in urinary crystals[5,29] and stones,[30] it is often present in *in vitro* synthesis.[31] The structure solved by Basso et al.[24a] was used as starting geometry for simulations involving the COT phase.

The calculated parameters for COM, COD and COT show good agreement with the experimental data, as it can be seen in **Table 1**. PBE–D2 approach shows better results in comparison with experimental values, than those obtained using PBE–D3. However, the structures of calcium oxalate polyhydrates can be adequately modeled with both methods, with a preference for the former, probably due to the strong ionic character of the crystal (i.e. the presence of Ca^{2+} and $C_2O_4^{2-}$ ions).

Spectroscopic analysisIR spectra

In **Figure 2** we compare the experimental (see experimental details) IR spectra measured at 4 K, with the calculated ones (PBE–D2). The spectra are normalized to the most intense peak. The theoretical spectra are obtained by fitting sums of Gaussian functions on the different calculated band intensities.

Whewellite - COM

The IR spectrum can be divided in three different zones of interest for its analysis (See **Table 2**). First, the **"**water region**"** in which 5 bands above 2900 $cm^{-1,}$ in room temperature experiments and even 6 considering the very broad pic around 3212 cm^{-1} in our experiment at very low temperature, whereas only four are calculated. As expected by Shippey,[32] and by Petrov et al.,[33] the missing line in the calculation is due to an overtone 2δ(HOH), and reinforced by Fermi resonance with one of the neighboring fundamental[33] bands which cannot be calculated in the harmonic approximation.

As expected by Conti et al.[34] propose than the δ(HOH) around 1600 cm^{-1} consist on 2 contributions. The first one very broad is associated to the δ(HOH) of the water strongly coupled with the motion of the oxalates molecules. Our calculations confirm this coupling between the water molecule 1 of the structure of Daudon et al.[17] and the oxalates molecules, which resulted in wavenumbers between 1591 cm^{-1} and 1623 cm^{-1}. This result is in very good agreement with the broad peak observed experimentally around 3212 cm^{-1} (supposed to be 2δ(HOH)). The second contributions are a medium weak band proposed by Conti et al.[34] being assigned to δ(HOH) of the more localized water molecule 2 of Daudon et al..[17] In our calculations, the wavenumbers around 1637 cm^{-1} were associated to the δ(HOH) of both water molecules together, and not only of water molecule 2. Nevertheless no implication of the oxalate ion has been observed. This calculated wavenumber fits very well with the main overtone 2δ(HOH) measured around 3268 cm^{-1}.

The second and third zones cover respectively the broad ν(CO) region around 1400 cm^{-1}, and the low wavenumber region between 1000 and 500 cm^{-1}, corresponding to the different COO vibrations (wagging, stretching and bending). The calculated vibrational spectrum is in agreement with experiment from Shippey[32] and Petrov et al.,[33] except for some small expected band shifts due to the calculation level

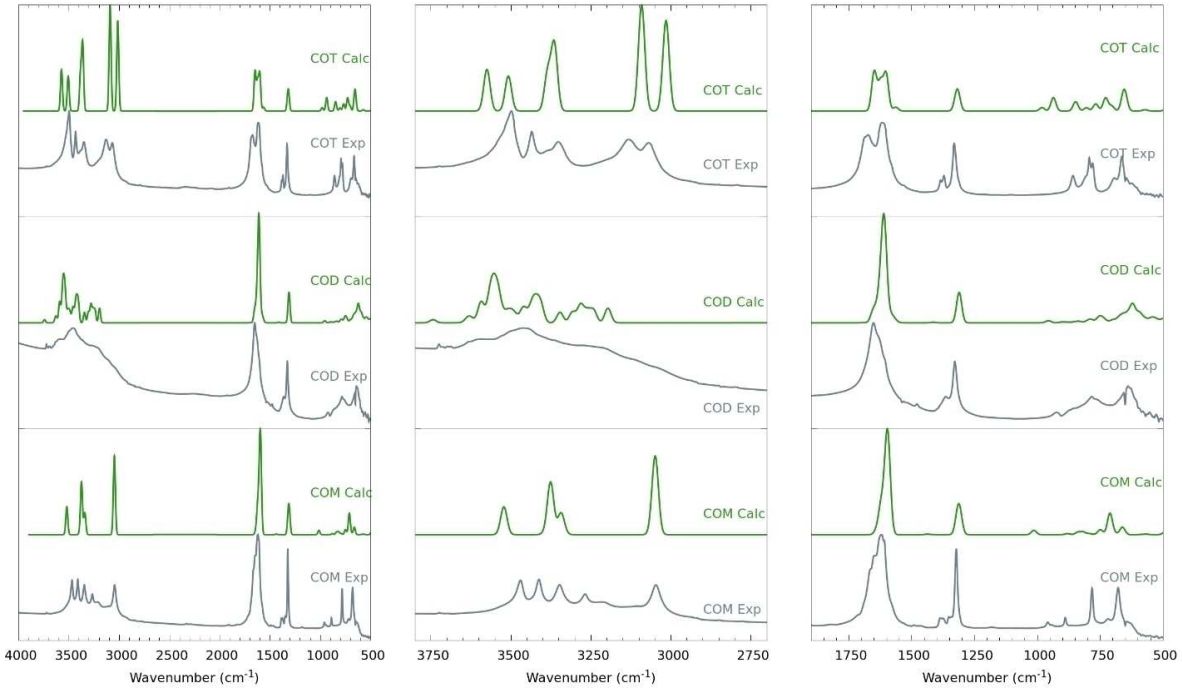

Figure 2. Experimental (gray) and calculated (green) IR spectra for the three calcium oxalate polyhydrates between: 500 and 4000 cm^{-1} for the theoretical spectrum and between: 600 et 4000 cm^{-1} for the experimental one. From left to right: total spectra, spectra between: 3800–2500 cm^{-1} and spectra between: 1900–500 cm^{-1}).

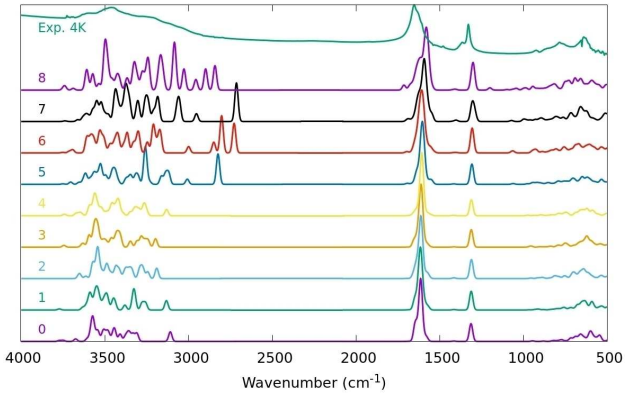

Figure 3. Calculated COD IR-spectra for unit cells with 0–8 extra water molecules (x = 0 to 1) and different configuration of zeolitic water molecules within the crystal, compared with the experimental IR spectrum at 4 K.

used. A point raised in the Shippey study concerned the different H-bonds present in whewellite, which were calculated from our optimized whewellite structure. The following H-bond distances were determined: H_2O–Ox along c-axis: 2.638 and 2.713 Å; H_2O-H_2O 2.786 Å; H_2O–Ox along b-axis: 2.899 - 2.899 Å.

In general, a small but significant redshift compared with the experimental spectrum which is attributed to the use of DFT (PBE–D level), which slightly overestimates H-bond interactions, such as those between the oxalate and calcium ions with the neighboring water molecules.

Weddellite - COD

The calculated IR spectrum for weddellite is able to predict, within the experimental error, all bands. The same very small redshift due to the accuracy of the calculation level is observed. The characteristic carbonyl symmetric stretching (exp.: 1589–1578 cm^{-1}) is clearly recovered (theor.: 1689–1539 cm^{-1}), and predicted to be the most intense band, which is in agreement with the experimental spectrum (See **Table 3**). The zone, between 3200–3700 cm^{-1}, corresponds to the O–H elongation of the water molecules. The identification of the vibration modes from the calculation presented in **Table 3** shows that several vibrational combinations are involved. This is due to the large hydrogen bond network between the water molecules, and between water and oxalate entities. The experimental spectra show a very broad band in this range, due to the presence of mobile zeolitic water in the COD unit cell, in contrast with COM. The mobility of the water molecules in the channels lead to a broader set of conformations and thus a broader range of which vibrations, making it difficult to interpret the part of the spectrum.

In order to investigate possible phase transitions or changes in the degree of hydration, which are related to the x parameter of weddellite, we calculated the IR spectra for x values between 0 to 1 (corresponding to 0 and 8 extra water molecules per unit cell). The spectra are presented in **Fig 3**. We show that for 5 water molecules or more per unit cell, intense bands around 2800 cm^{-1} appear on the calculated spectra but are not present in the experimental spectrum suggesting that

Table 2. PBE–D2 calculated whewellite IR wavenumbers corresponding to the different types of vibration (in cm^{-1}): a-antisymmetric, s-symmetric, ν-stretching, δ-bending, L-libration, R-rocking, W-wagging, and T-twisting. Next to the wavenumbers the intensity is given by: s-strong, v-very, m-medium, w-weak, b-broad, and sh-shoulder.

Present work			Literature [22,32–33,35]
Theor. band	Exp. band	Assignment	Assignment
3531 – 3521	3470 m, sh	ν_a(OH)	ν(OH)
3395 – 3376	3412 m, sh	ν_a(OH)	ν(OH)
3344 – 3338	3347 m	ν_s(OH) H bonds between water	ν(OH)
	3268 w, 3212 w		2δHOH
3055 – 3047	3046 m, b	ν_a(OH) a strong H bond with CO	ν(OH)
	2937 w, sh		combination
1649	1665 vs, sh	ν_a(CO)	δHOH
1639 – 1635	1648 w	δ(HOH)	
1623 – 1591	1620 vs	ν_a(CO) + δ(HOH)	
	1581 w, sh	ν_a(CO)	ν_a(CO)
	1487 w		
	1462 w		ν_s(CO)
1439 – 1432		ν_s(CO) AC plane	
1415 – 1413		ν_s(CO) AB plane	
	1386 m		combination
	1374 w, sh		combination
	1353 w		
1325 – 1320	1344 w	ν_s(CO) AC and BC plane	
1318 – 1315		ν_s(CO) AC	
1308	1322 vs	ν_s(CO) BC plane	ν_s(CO)
1017 – 1010	958 w, b 943 w	L	L–R(H_2O)
881 – 879	889 m	ν(CC) in AC place + L(HOH)	L–R(H_2O)
871 – 869		ν(CC) in BC place	L
842 – 825	863 w	L–W(OCO) in AC plane + L (HOH)	ν(CC)
824 – 823		L–W(OCO) wagging BC	
819 – 817		L–W(OCO) BC and AC + L (HOH)	
794 – 785		δ(OCO) AC + L–R(HOH)	
	782 s		δOCO
761 – 749		δ(OCO) BC + L–R(HOH)	
717 – 690	719 w	δ(OCO) L–R(HOH)	
678 – 661	678 s	L- R W (HOH)	L(HOH)
589 – 588		L–R(OCO) a in AC	
579 – 576		L–R(OCO) a in BC	
568 – 563		L–R(HOH)	
510 – 507		ν(CC) AC	
500 – 502		ν(CC) BC	
490		L–W(OCO) BC	
487		L–W(OCO) BC	
486		L–W(OCO) AC	
below 314		Ca implicated vibrations	

Table 3. PBE–D2 calculated IR wavenumbers for the different weddellite vibrational modes (in cm^{-1}): a-antisymmetric, s-symmetric, ν-stretching, δ-bending, L-libration, R-rocking, W-wagging, and T-twisting. Next to the wavenumbers the intensity is given by: s-strong, v-very, m-medium, w-weak, b-broad, and sh-shoulder.

Present work			Literature [22,35–36]
Theor. band	Exp. band	Assignment	Assignment
3758 – 3719		ν_a(OH)	
3676 – 3644		$\nu_{a,s}$(OH)	
3623 – 3614		ν_a(OH) (close to carboxylic group)	
3602 – 3452		ν_a(OH) (close to water)	
	3559-3257 m, vb		ν(OH)
3442 – 3439		ν_s(OH)	
3426		ν_a(OH) (close to water)	
3379 – 3249		ν_a(OH) (close to carboxylic group)	
3226 – 3054		ν_a(OH) (close to water)	
2896	2939 vw, sh	ν_a(OH) (with strong H-bond)	combination
	2785 vw, sh		combination
1686 – 1539	1640 vs	ν_a(CO)	ν_a(CO)
	1475 w		ν_s(CO)
1429 – 1304	1363 w, sh	ν_s(CO)	combination
	1319 vs		ν_s(CO)
1060		L–T (HOH)	
966 – 905		L (HOH)	
898 – 860	915 w	ν_s(CO) + L(H_2O)	
853 – 825		L–W(OCO) + L(HOH)	
800 – 700	770 s, b	δ(OCO) + L(HOH)	δ(OCO)
700 – 620	630 m,sh	L(HOH)	
607 – 568		L–R(OCO) + L(HOH)	
549 – 521		L–R(HOH)	
516 – 400		L–W(OCO) + L(OHO)	
Below 400		Ca implicated vibrations	

the weddellite does not contain more than 4 zeolitic water molecules per unit cell. This result agrees with the calculated adsorptions energies[50]. For the structures having between 0 and 4 (x = 0 – 0.5) water molecules, the IR spectra are quite similar and in good agreement with the experimental one.

Caoxite - COT

The calculated IR spectrum for caoxite presents a good agreement with the experiment (See **Table 4**). The main difference is the relative intensity between the "water" bands above 2900 cm^{-1} and the CO/CC band around 1700 cm^{-1}. This inversion in intensity might be due to the dehydration process of the experimental phase. On the basis of the calculated spectra, the assignments for all bands are proposed (See **Table 4**).

Table 4. PBE–D2 calculated caoxite IR wavenumbers corresponding to the different types of vibration (in cm^{-1}): a-antisymmetric, s-symmetric, ν-stretching, δ-bending, L-libration, R-rocking, W-wagging, and T-twisting. Next to the wavenumbers the intensity is described as: s-strong, v-very, m-medium, w-weak, b-broad, and sh-shoulder.

Present work			Literature[11,22,35]
Theor. band	Exp. band	Assignment	Assignment
3575 – 3574	3551 m, 3466 s, sh	ν_a(OH) close to carboxylic group	ν(OH)
3508 – 3505	3436 m	ν_a(OH) close to H_2O	ν(OH)
3385 – 3382	3385 w	ν_a(OH) close to H_2O	
3370 – 3364	3355 m	ν_a(OH) close to carboxylic group	
3103 – 3015	3132 m, b, 3067 m	ν_a(OH) close to carboxylic group	ν(OH) with strong H band
	2936 vw, sh		Combination
	2785 vw, sh		Combination
1667 – 1616	1679 s, sh	δ(HOH) + ν_a(CO)	δ(HOH)
1603 – 1602	1616 vs	ν_a(CO)	ν_a(CO)
1564 – 1562		δ(HOH) + ν_a(CO)	
1420 – 1424	1386 w 1372 w	ν_s(CO)	Combination
1322 – 1315	1316 vs	ν_s(CO)	ν_s(CO)
993 – 981		L–R (HOH)	
937 – 936		L–W (HOH)	
893 – 882		δ(OCO)	
857 – 848		L- W(HOH)	
834		L- W(OCO)	
831	859 w, sh	L–W (HOH)	L-(HOH)
828		L–W(OCO)	
822		L–W(OCO) + L–R(HOH)	
794 – 598	794 s	L–R (HOH)	δ(OCO)
	779 s, 664 s,b		
485 – 471		L–T(OCO)	
430 – 395		δ(OCO)	
332 – 0		Ca implicated vibrations	

Raman spectra

Raman spectroscopy is a highly reliable technique for the identification of the different Ca oxalate polyhydrates in kidney stones. Previous reports[37] show accurate and reliable Raman spectral identification assignment, e.g. COM can be easily identified from the other ones, if two strong bands appear at ~1489 cm^{-1} and ~1462 cm^{-1} (in that region, COD and COT show just one band).

In **Figure 4** we compare the experimental Raman spectra, with the calculated ones (PBE–D3) obtained by fitting sums of Gaussian functions on the different calculated band intensities. The spectra are normalized to the most intense band.

Whewellite - COM

The Raman spectra, similarly to the IR spectra, can be divided in three zones: the "water" region (3600 - 3000 cm^{-1}), the CO and CC stretching zone (1650 - 1350 cm^{-1}), and the low wavenumbers zone (1000 - 10 cm^{-1}).

In **Table 5** the theoretical Raman bands for whewellite have been reported, and compared with the experimental results of ref.,[34] which are comparable to our experimental Raman data. Five bands corresponding to symmetric and asymmetric OH vibrations of H_2O molecules are observed in the first zone, in agreement with those reported by Conti et al..[34] The oxalate vibrations in different planes (the perpendicular ab and bc planes), and a vibration synchronism with the oxalate nearest neighbor occur around 1500 cm^{-1}. These bands appear shifted to higher wavenumbers in our calculations. Low wavenumbers zone below 1000 cm^{-1} correspond to different OCO vibrations, water vibrations and lattice vibrations where Ca is involved. Around 900 cm^{-1}, bending OCO vibrations are observed. Lattice vibrations which involved Ca ions are below 330 cm^{-1}, and for an easiest identification CaO_2Ca rhombus structures have been established (**Figure 5**).

It is interesting to note that the agreement of the calculated spectrum with the experimental one between 1700 and 400 cm^{-1} is particularly good, except for some small expected band shifts and intensities.

Weddellite - COD

The calculated weddellite Raman spectra predict relatively well our experimental results and are in agreement with the reported data, except for some small band shift differences.[35,38] **Table 6** shows the results for the calculated spectra and their comparison with the experimental assignation of Frost et al..[38] The same regions described for COM can be identified. Between 3500–3200 cm^{-1} experimental results show only a broad band, but in our theoretical results multiple and narrow peaks of OH stretching are observed because of the nature of the calculation at low temperature. Between 1470–1370 cm^{-1}, we observe just one broad peak at 1425 cm^{-1}, that can corresponds to the overlap of the strong ν_a(CO) band with the ν_s(CC) + δ(OCO) vibration bands which is indicated around 1475 cm^{-1} in ref..[34] Additionally, it is important to note that water vibrational bands are coupled with those of the oxalates and Ca below 900 cm^{-1}. For a better description of these vibrations, CaO_2Ca rhombus structures have been identified and shown in **Figure 5**.

Caoxite - COT

The Raman spectrum for caoxite exhibits the same three distinguishable zones, which have been described for COM and COD spectra. The assignment of bands in the calculated Raman spectrum and its comparison with previous experimental results[34] are presented in **Table 7**. Our theoretical results show small shifts in the bands around 1470 cm^{-1} with respect to the experimental ones.

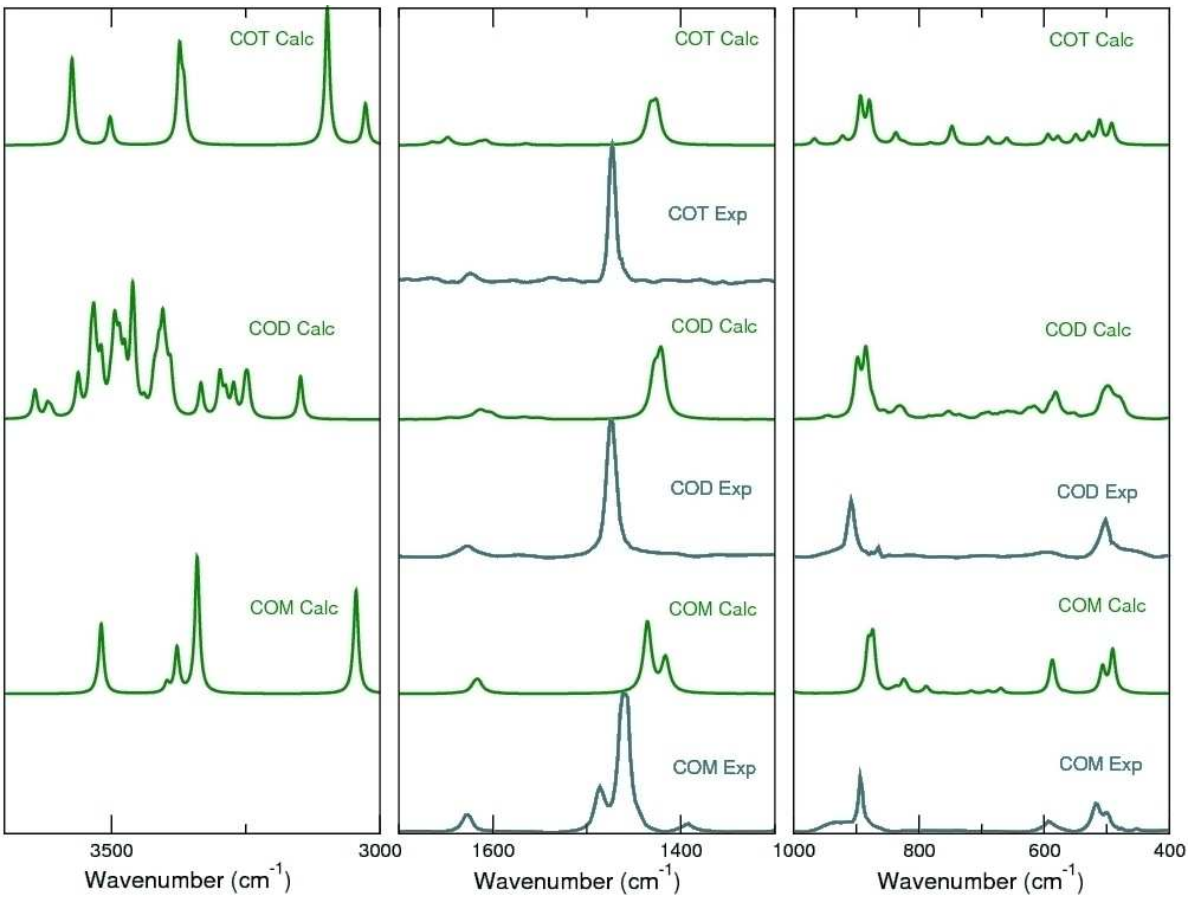

Figure 4. Experimental (gray) and calculated (green) Raman spectra for the three calcium oxalate polyhydrates obtained between 4000 and 400 cm^{-1}. Three spectra regions are shown when possible for comparison. From left to right: between 3600–3000 cm^{-1}, 1700–1300 cm^{-1} and 1000–400 cm^{-1} .

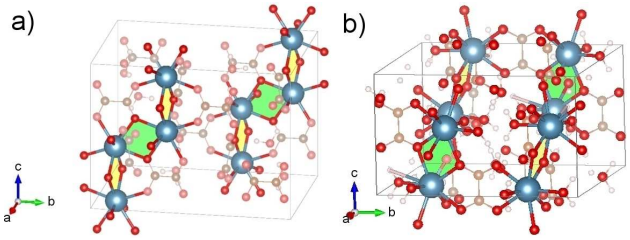

Figure 5. The corresponding CaO_2Ca rhombus structures in AC plane (yellow) and BC plane (green) for (a) COM and (b) COD.

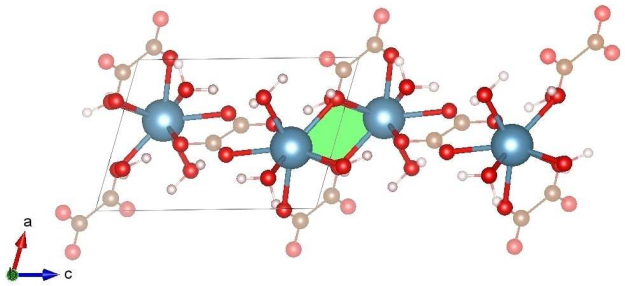

Figure 6. Corresponding CaO_2Ca rhombus structure for COT as discussed in **Table 7**.

In the CO and CC stretching zone between 1000 and 500 cm^{-1}, we find the vibration of OCO bending and some vibrations corresponding to water molecules. The zone of low wavenumbers (below 1000 cm^{-1}) presents a band profile similar to COM but with different band positions, which is characteristic for each calcium oxalate polyhydrates. It is interesting to note that water vibrations are important in this region. A detailed description is presented in **Table 7**, which until now and to the best of our knowledge was not carried out in previous works. For a better analysis, the particular COT structure allows us to define only a CaO_2Ca rhombus structure, as seen in **Figure 6**. In addition, the differences of the bands between COT and the other polyhydrates will be discussed below.

In the interesting work of Conti et al.[35] discussing the normal modes of the oxalate ion with average geometry, 2 vibrational modes are still missing. To complete the list of

Table 5. PBE–D3 calculated whewellite Raman modes wavenumbers (in cm^{-1}) and assignment with the type of vibration: a-antisymmetric, s-symmetric, ν-stretching, δ-bending, L-libration, R-Rocking, W-wagging, and T-Twisting. The measured mode wavenumbers are reported as: s-strong, v-very, m-medium, w-weak, and b-broad.

Present work			Literature[35]
Theor. band	Exp. band	Assignment	Assignment
3610 – 2970		OH stretching bands	ν(OH)
3610 – 3450	3486 w	ν_a(OH)	
3410 – 3390	3426 m	ν_a(OH)	
3390 – 3360	3340 w	ν_a(OH)	
3360 – 3260	3256 w	ν_s(OH)	
3110 – 2970	3056 w	ν_s(OH)	
1645 – 1585	1629 m	ν_a(CO)	ν_a(CO)
1478 – 1380		ν_s(CC) + ν_s(CO)	
1478 – 1423	1490 vs 1463 vs	ν_s(CC) + ν_s(CO) on AC plane, asym vibr with nearest neighb.	ν_s(CC) + ν_s(CO)
1423 – 1380	1396 m	ν_s(CC) + ν_a(CO) on BC plane, asym vibr with nearest neighb.	ν_s(CC) + ν_s(CO)
1040 – 990	942 w b	δ(OCO) on AC plane + L–W(HOH)	
927 – 850		ν(CC) + δ(OCO) + L–W (HOH)	
879	896 s	ν(CC) + δ(OCO) on BC plane, sym vibr with nearest neighb. + L–W(HOH)	ν(CC) + L–W(HOH)
874	863 m	ν(CC) + δ(OCO) on AC plane, sym vibr with nearest neighb. + L–W(HOH)	ν(CC) + L–W(HOH)
850 – 804		L–W(OCO)	
839		L–W(OCO) on AC plane + L(HOH)	
825		L–W(OCO) on BC plane	
800-645		δ(OCO) + L(HOH)	
785		δ(OCO) in AC plane, asym vibr with nearest OCO + L–R(HOH)	
753		δ(OCO) in BC plane, asym vibr with nearest OCO + L (HOH)	
740 – 645		δ(OCO) + L(HOH)	
625 – 545	597 m	L–R(OCO) on AC and BC plane, asym vibr with nearest neighb.	
506 – 435		ν(CC) + ν(Ca–O)	
506	522 m	ν(CC) + ν(Ca–O) in AC plane	
490	503 s	ν(CC) + ν(Ca–O) in BC plane	
below 326		Lattice vibration in which Ca is implicated	
292		$\nu_s(CaO_2)$ on CaO_2Ca rhombus structure in AC plane + L(HOH)	
256		$\nu_s(CaO_2)$ on CaO_2Ca rhombus structure in AC and BC plane	Elongation/ compression of Ca opposite vertices on CaO_2Ca rhombus structure + L(HOH)
224		$\nu_s(CaO_2)$ on CaO_2Ca rhombus structure in BC plane	
205		$T(CaO_2)$ on CaO_2Ca rhombus + L(HOH)	

vibrations we attempted to add the missing B_{2g} mode. It was concluded that this mode might be coupled with the B_{1u} mode (not observed), showing vibrations wavenumbers for the oxalate ions in one plane (ac plane) of ~838 cm^{-1} and ~825 cm^{-1} for the other plane (bc plane), which are thus mixed with vibrations of the water molecules.

Identification of the low wavenumber Raman bands

There is not much information about band assignment in the low wavenumber Raman region, because of the existence of both, coupled and lattice vibrations. According to our theoretical results and to shed light on possible deeper characterizations leading to new analysis methodologies, detailed assignments are displayed in **Figure 7**, and **Tables 5, 6** and **7**. The pattern of the theoretical spectra do not completely fit the experimental ones, especially the intensities of some bands are not completely well reproduced, which might be caused by the shape of the oxalate particles.

Our results show that around 890 cm^{-1}, the COM bands are found at lower wavenumbers than the bands of the other polyhydrates, due to CC stretching and OCO bending. For COD and COT, two easily distinguishable bands are observed, while for COM the bands are strongly overlapping. Previous experimental results[34] are in agreement with ours, although a single band for the three cases was found, which could be due to experimental issues, such temperature and instrumental broadening.

The correct assignment of the Raman bands observed between 600–490 cm^{-1} help us to identify the calcium oxalate polyhydrates because this region presents a particular profile for each one. The bands correspond to vibrations in which water, oxalate and Ca ions are involved. The band of high intensity for that zone is found at the following wavenumbers: COM (~ 490 cm^{-1}), COD (~ 498 cm^{-1}) and COT (~ 511 cm^{-1}),

Table 6. PBE–D3 calculated weddellite Raman wavenumbers corresponding to the different types of vibration (in cm^{-1}): a-antisymmetric, s-symmetric, ν-stretching, δ-bending, L-libration, R-rocking, W-wagging, and T-twisting. For some signals, the intensity is reported next to the wavenumbers as: s-strong, v-very, m-medium, w-weak, and b-broad.

Present work Theor. band	Exp. band	Assignment	Literature[38] Assignment
3750 – 3110	3500 – 3200 b	OH stretching bands	ν(OH)
3740		ν_a(OH)	
3643 – 3619		ν_s(OH)	
3565 – 3462	3467	ν_a(OH)	ν(OH)
3450 – 3412		ν_s(OH)	
3407		ν_a(OH)	
3393 – 3248	3266	ν_a(OH)	ν(OH)
3149		ν_a(OH)	
1658 – 1540		ν_a(CO)	ν_a(CO)
1613	1623 w	ν_a(CO)	ν_a(CO)
1603	1605	ν_a(CO)	ν_a(CO)
1470 – 1370	1475 vs 1411 b	ν_s(CC) + ν(CO) + δ(OCO)	-ν_a(CO) + ν_s(CC) + δ(OCO)s
896	909 s	ν_s(CC) + δ(OCO) + L–W (HOH)	ν_s(CC) + δ(OCO) + L–W (HOH)
883	868 vw	ν_s(CC) + δ(OCO) + L–W (HOH)	ν_s(CC) + δ_s(OCO) + L–W (HOH)
829		W(OCO) + L–R(HOH)	water rocking
753		δ(OCO) + L–R(HOH)	
725 – 680		L–R(HOH) + L–W(HOH)	
680 – 638		δ(OCO) + ν_s(CC)	
600 – 540	596 vw, b	L–R(OCO) + L(HOH)	L–R(OCO) + L(HOH)
616		L(HOH)	
580		L–R(OCO) + L(HOH)	
Below 540		Lattice vibration with Ca implicated	
540 – 430	505	ν_a(Ca–O) + ν_s(CC) + L (HOH)	ν_a(Ca–O) + ν_s(CC) and water vibration L(HOH)
498		ν_a(Ca–O) on CaO_2Ca rhombus structure in BC plane + ν_s(CC) + L(HOH)	
480		ν_a(Ca–O) on CaO_2Ca rhombus structure in AC plane + ν_s(CC) + L(HOH)	
301	259	L–W(CaO_2) on CaO_2Ca rhombus structure + L–T (OCO) in AC plane + L (HOH)	L–W(CaO_2) on CaO_2Ca rhombus structure + L–T (OCO) in AC plane + L (HOH)
253		ν_s(CaO_2) on CaO_2Ca rhombus structure in AC plane + L–R(OCO) + L(HOH)	
228	220	ν_s(CaO_2) on CaO_2Ca rhombus structure in BC plane + L–R(OCO) + L(HOH)	Elongation/ compression of Ca opposite vertices on CaO_2Ca rhombus structure + Oxalate and water vibrations
210	188	L–T(CaO_2) on CaO_2Ca rhombus structure in BC plane + L–T(OCO) + L (HOH)	L–W(CaO_2) on CaO_2Ca rhombus structure in BC plane + L–T(OCO) + L (HOH)

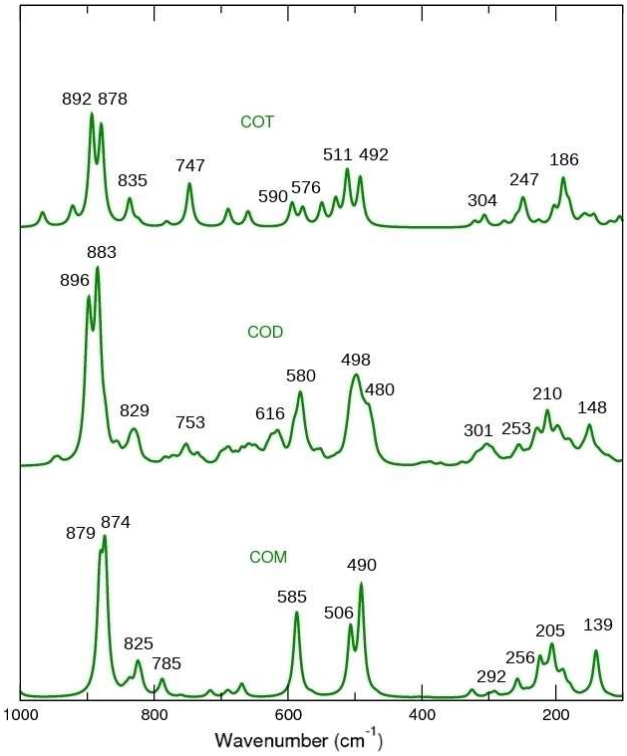

Figure 7. Low wavenumber region: comparison between the theoretical Raman spectra of COM, COD and COT obtained between 1000 and 10 cm^{-1}.

which correspond to the experimental bands:[34] 503, 506 and 507 cm^{-1} respectively. Interestingly, the trend observes with experimental data is respected through our DFT calculations despite the slightly shifted values.

Another important region is between 300–10 cm^{-1}, where other specific water molecules, oxalate and Ca ions are detected. The band around 200 cm^{-1} allows to distinguish between COM (~ 205 cm^{-1}), COD (~ 210 cm^{-1}) and COT (186 cm^{-1}). That band includes torsional vibration bands of CaO_2 groups coupled with water and OCO torsional vibrations that have a vibration mode that is symmetric with the other OCO, which forms the oxalate ion (**Figure 8a**). In addition, the

Table 7. PBE–D3 calculated caoxite Raman wavenumbers corresponding to the different types of vibration (in cm^{-1}): a-antisymmetric, s-symmetric, ν-stretching, δ-bending, L-libration, R-rocking, W-wagging, and T-twisting. Next to the wavenumbers, the intensity is reported as: s-strong, v-very, m-medium, w-weak, and b-broad.

Present work Theor. band	Exp. band	Assignment	Literature[35] Assignment
3625 – 3000	3500 – 3200 b	OH stretching band	ν(OH) Bands
3625 – 3530		ν_s(OH)	
3520 – 3475		ν_a(OH)	
3400 – 3330		ν_s(OH)	
3125 – 3065	2941 m	ν_a(OH)	ν(OH)
3055-3000	2882 w	ν_a(OH)	
1680 – 1550	1668 w, b	δ(HOH) + ν_a(CO)	
1664		δ(HOH) + ν_a(CO) in BC plane	
1648		δ(HOH) + ν_a(CO)parallel and perpendicular to BC plane	
1607		δ(HOH) + ν_a(CO)perpendicular to BC plane	
1564		δ(HOH) + ν_a(CO) on BC plane	
1500 – 1355	1472 vs 1418 b	ν_s(CC) + ν_s(CO) perpend to BC plane	ν_s(CC) + ν_s(CO)
995 – 948		[ν_s(CC) + ν_s(CO)] on BC plane + L (HOH)	
940 – 910	912 s	[ν_s(CC) + ν_s(CO)] on BC plane + L (HOH)	ν_s(CC) + ν_s(CO) + L (HOH)
892		[ν_s(CC) + δ(OCO)] perpendicular to BC plane + L–W (HOH)	
878	867 m, s	[ν_s(CC) + δ(OCO)] on BC plane + L–W(HOH)	ν_s(CC) + δ(OCO) + L–W(HOH)
835		L–W(OCO) parallel and perpendicular to BC plane + L–T (HOH)	
747	582 w, b	L–R(HOH)	L (HOH) water rocking
601 – 565		L–R(OCO)	
590		L–R(OCO) parallel to the BC plane	
576		L–R(OCO) perpend to the BC plane	
565 – 520		L–T(HOH)	
520 – 465		ν(Ca–O) + ν_s(CC)	
511	507 s	ν(Ca–O) + ν_s(CC) perpendicular to BC plane	tentatively assign L–R (OCO).[35]
492		ν(Ca–O) + ν_s(CC) on BC plane	
Below 335		Lattice vibration with Ca implication	
304		ν_s(CaO_2) on CaO_2Ca rhombus + L–R(OCO) + L(HOH)	
247		ν_a(CaO_2) on CaO_2Ca rhombus + L–R(OCO) + L(HOH)	Elongation/ compression of Ca opposite vertices
203		L–T(CaO_2) on CaO_2Ca rhombus + L–R(OCO) + L(HOH)	
186		L–T(CaO_2) on CaO_2Ca rhombus + L–T(OCO) + L(HOH)	

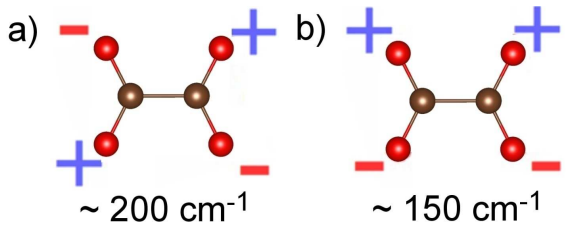

Figure 8. Oxalate vibrations observed at low wavenumbers region (+ increase of bond length, - decrease of bond length).

other OCO torsional vibrations that have an asymmetric vibration with the next one in the ion (**Fig. 8b**), coupled with CaO_2 torsional vibrations, are observed as a singular peak at ~ 139 cm^{-1} or 148 cm^{-1} for COM and COD, respectively.

This assignments can be confirmed and with good agreement with the previous experimental work reported by Conti et al.[34]

Comparison between oxalic acid and Ca oxalate mono and di hydrate

Although, the small probability of the presence of the acidic oxalate form, its spectrum was investigated. Due to its low first pKa around 1.2, it is not expected to be present in the synthetic samples, nevertheless this cannot be said with certainty for natural samples. So, for the sake of comparison we calculated the Raman spectrum of the oxalic acid. It is interesting to note that if oxalic acid would form during the synthesis of Ca oxalates, it could be clearly distinguished from its Ca salt counterparts. The theoretical Raman spectrum of oxalic acid dihydrate has been obtained and compared with an experimental one (see **Figure 9**). Calculated Raman spectrum predicts well the experimental results, and it is in good agreement with previous studies.[39]

Only the signal at 1750 cm^{-1} (corresponding to the CO stretch band) shifts slightly at higher wavelengths in the theoretical spectrum. This band shows the presence of oxalic acid, since it is absent in the calcium oxalates COM and COD, the most common polyhydrates found in kidney stones. According to these results, it is expected that if oxalic acid is present in natural samples, it can be easily detected and

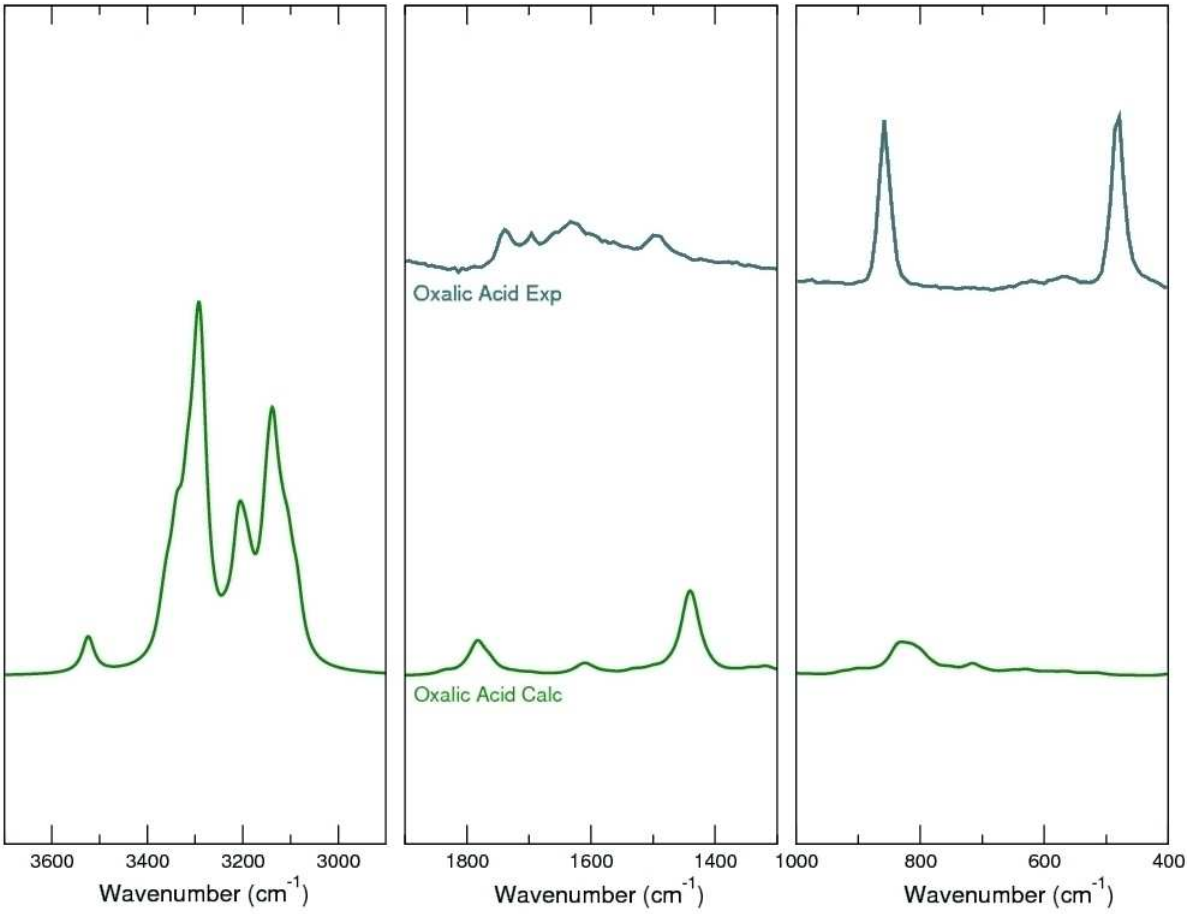

Figure 9. Comparison between the theoretical and experimental Raman spectrum of dihydrate oxalic acid.

quantified. As expected, in our samples we conclude that no oxalic acid is present.

Conclusions

DFT calculations performed on the calcium oxalate polyhydrate unit cells were used to investigate the vibrational bands measured by Raman and IR spectroscopies. Most bands were assigned and the theoretical predictions were compared when possible with available experimental data, for both, IR and Raman spectroscopies. Such an approach allowed a more accurate analysis of vibrational spectra helping in the completion of the assignments of the vibrational bands of the three calcium oxalate polyhydrates.

The IR spectra of COM and COT were very well reproduced. Due to the presence of zeolitic water molecules in the COD structure, a systematic study on the x parameter in $CaC_2O_4{\cdot}(2+x)\ H_2O$ was undertaken. By calculation of the different spectra for $x=0-1$ we showed that the typical x-value is equal to three, which corresponds to the degree of hydration found in the experimental samples. Moreover, we were able to present several distributions for the water molecules in the channels of COD structure, which motivated us to start to unravel thoroughly the water structure at the molecular level, combining spectroscopic techniques and ab initio calculations. We concluded that the channel available for water adsorption is filled with a maximum of two to three water molecules per unit cell (one channel with two and another with one water molecule).

The Raman spectra for the three calcium oxalate polyhydrates were calculated and completely resolved, which is expected to facilitate the characterization of the calcium oxalate polyhydrates in natural samples.

It has been paid special attention to the low wavenumber Raman active vibrations and the vibrations of oxalic acid. The low vibrational modes in the Raman spectrum are of importance in the identification of the different oxalate polyhydrates, whereas the oxalic acid was studied to investigate its presence in the experimental samples. A theoretical spectrum of oxalic acid was discussed and compared with the calcium polyhydrate forms.

Supporting Information Summary

The computational details including the calculation level and the information on the vibrational spectrum calculations, as well as the experimental details concerning the origin of the

samples and the technical details of the experiments are presented in the Supporting Information.

Acknowledgements

The French state funds managed by the ANR within the Investissements d'Avenir programme under reference ANR-11-IDEX-0004-02, and more specifically within the framework of the Cluster of Excellence MATISSE led by Sorbonne Université. HPC resources from GENCI-[CCRT/CINES/IDRIS] (Grant 2016-[x2016082022]) and the CCRE of Université Pierre et Marie Curie are also acknowledged.

Conflict of Interest

The authors declare no conflict of interest.

Keywords: Calcium oxalate · DFT · IR · polyhydrates · RAMAN

[1] a) C. Krafft, V. Sergo, *Spectr.: Int. J.* **2006**, *20*, 195–218; b) M. Pilling, P. Gardner, *Chem. Soc. Rev.* **2016**, *45*, 1935–1957.
[2] F. Severcan, P. I. Haris, *Vibrational Spectroscopy in Diagnosis and Screening, Vol. 6 of Advances in Biomedical Spectroscopy*, IOS press ed., **2012**.
[3] a) F. Le Naour, M.-P. Bralet, D. Debois, C. Sandt, C. Guettier, P. Dumas, A. Brunelle, O. Laprevote, *Plos One* **2009**, *4*; b) F. Le Naour, C. Sandt, C. Peng, N. Trcera, F. Chiappini, A.-M. Flank, C. Guettier, P. Dumas, *Anal. Chem.* **2012**, *84*, 10260–10266.
[4] M. J. Baker, J. Trevisan, P. Bassan, R. Bhargava, H. J. Butler, K. M. Dorling, P. R. Fielden, S. W. Fogarty, N. J. Fullwood, K. A. Heys, C. Hughes, P. Lasch, P. L. Martin-Hirsch, B. Obinaju, G. D. Sockalingum, J. Sule-Suso, R. J. Strong, M. J. Walsh, B. R. Wood, P. Gardner, F. L. Martin, *Nat. Prot.* **2014**, *9*, 1771–1791.
[5] M. Daudon, V. Frochot, D. Bazin, P. Jungers, *C. R. Chim.* **2016**, *19*, 1514–1526.
[6] N. Quy Dao, M. Daudon, *Infrared and Raman Spectra of Calculi.*, **1997**.
[7] A. Lionet, M. Haeck, A. Garstka, V. Gnemmi, D. Bazin, E. Letavernier, J.-P. Haymann, C. Noel, M. Daudon, *C. R. Chim.* **2016**, *19*, 1542–1547.
[8] a) A. Dazzi, C. B. Prater, *Chem. Rev.* **2017**, *117*, 5146–5173; b) D. Bazin, M. Daudon, *Ann. Biol. Clin.* **2015**, *73*, 517–534.
[9] M. Daudon, O. Traxer, P. Conort, B. Lacour, P. Jungers, *J. Am. Society of Nephrol.* **2006**, *17*, 2026–2033.
[10] M. Daudon, *Épidémiologie actuelle de la lithiase rénale en France, Vol. 39*, Elsevier, **2005**.
[11] T. Echigo, M. Kimata, A. Kyono, M. Shimizu, T. Hatta, *Mineralogical Magazine* **2005**, *69*, 77–88.
[12] H. Colas, L. Bonhomme-Coury, C. C. Diogo, F. Tielens, F. Babonneau, C. Gervais, D. Bazin, D. Laurencin, M. E. Smith, J. V. Hanna, M. Daudon, C. Bonhomme, *CrystEngComm* **2013**, *15*, 8840–8847.
[13] H. J. Arnott, F. G. E. Pautard, H. Steinfink, *Nature* **1965**, *208*, 1197-+.
[14] V. Tazzoli, C. Domeneghetti, *Am. Miner.* **1980**, *65*, 327–334.
[15] O. Hochrein, A. Thomas, R. Kniep, *Z. Anorg. Allg. Chem.* **2008**, *634*, 1826–1829.
[16] a) S. Deganello, *Z. Kristallogr.* **1980**, *152*, 247–252; bS. Deganello, *Acta Crystallogr., Sect. B: Struct. Sci.* **1981**, *37*, 826–829.
[17] M. Daudon, D. Bazin, G. Andre, P. Jungers, A. Cousson, P. Chevallier, E. Veron, G. Matzen, *J. Appl. Crystallogr.* **2009**, *42*, 109–115.
[18] C. Sterling, *Science* **1964**, *146*, 518-&.
[19] C. Sterling, *Acta Crystallogr.* **1965**, *18*, 917-&.
[20] A. R. Izatulina, V. Y. Yelnikov, *Structure, chemistry and crystallization conditions of calcium oxalates - The main components of kidney stones*, Springer Nature Switzerland AG., **2008**.
[21] A. Izatulina, V. Gurzhiy, O. Frank-Kamenetskaya, *Am. Miner.* **2014**, *99*, 2–7.
[22] C. Conti, L. Brambilla, C. Colombo, D. Dellasega, G. D. Gatta, M. Realini, G. Zerbi, *Phys. Chem. Chem. Phys.* **2010**, *12*, 14560–14566.
[23] G. L. Gardner, *J. Cryst. Growth* **1975**, *30*, 158–168.
[24] aR. Basso, G. Lucchetti, L. Zefiro, A. Palenzona, *Neues Jahrb. Mineral., Monatsh.* **1997**, 84–96; bR. F. Martin, W. H. Blackburn, *Can. Miner.* **1999**, *37*, 1045–1078.
[25] S. Deganello, A. R. Kampf, P. B. Moore, *Am. Miner.* **1981**, *66*, 859–865.
[26] L. Walterlevy, J. Laniepce, *C. R. Hebd. Seances Acad. Sci.* **1962**, *254*, 296-&.
[27] a) B. Tomazic, G. H. Nancollas, *J. Cryst. Growth* **1979**, *46*, 355–361; b) B. B. Tomazic, G. H. Nancollas, *Invest. Urol.* **1980**, *18*, 97–101.
[28] a) B. Xie, T. J. Halter, B. M. Borah, G. H. Nancollas, *Cryst. Growth Des.* **2015**, *15*, 204–211; b) M. Hajir, R. Graf, W. Tremel, *Chem. Comm.* **2014**, *50*, 6534–6536.
[29] M. Daudon, R. J. Reveillaud, P. Jungers, *Lancet* **1985**, *1*, 1338–1338.
[30] W. Heijnen, W. Jellinghaus, W. E. Klee, *Urol. Res.* **1985**, *13*, 281–283.
[31] M. Daudon, in *Lithiase Urinaire* (Eds.: P. Jungers, M. Daudon, A. Le Duc), Flammarion Médecine-Sciences, Paris, France, **1989**, pp. 158–195.
[32] T. A. Shippey, *J. Molec. Struct.* **1980**, *63*, 157–166.
[33] I. Petrov, B. Soptrajanov, *Spectrochim. Acta Part a* **1975**, *A 31*, 309–316.
[34] C. Conti, M. Casati, C. Colombo, M. Realini, L. Brambilla, G. Zerbi, *Spectrochim. Acta Part a* **2014**, *128*, 413–419.
[35] C. Conti, M. Casati, C. Colombo, E. Possenti, M. Realini, G. D. Gatta, M. Merlini, L. Brambilla, G. Zerbi, *Spectrochim.Acta Part a* **2015**, *150*, 721–730.
[36] a) J. M. Ouyang, L. Duan, B. Tieke, *Langmuir* **2003**, *19*, 8980–8985; b) L. Maurice-Estepa, P. Levillain, B. Lacour, M. Daudon, *Clin. Chim. Acta* **2000**, *298*, 1–11.
[37] J. Tonannavar, G. Deshpande, J. Yenagi, S. B. Patil, N. A. Patil, B. G. Mulimani, *Spectrochim. Acta Part a* **2016**, *154*, 20–26.
[38] R. L. Frost, *Anal. Chim. Acta* **2004**, *517*, 207–214.
[39] a) V. Mohacek-Grosev, J. Grdadolnik, J. Stare, D. Hadzi, *J. Raman Spectrosc.* **2009**, *40*, 1605–1614; b) Y. Ebisuzaki, S. M. Angel, *J. Raman Spectrosc.* **1981**, *11*, 306–311.

Submitted: May 28, 2018
Accepted: July 30, 2018